

Effects of magnonic Kerr nonlinearity on magnon-polaritons with a soft-mode

Takahiro Chiba^{1,2, a)}

¹⁾Department of Information Science and Technology, Graduate School of Science and Engineering, Yamagata University, Yonezawa, Yamagata 992-8510, Japan

²⁾Department of Applied Physics, Graduate School of Engineering, Tohoku University, Sendai, Miyagi 980-8579, Japan

(Dated: 16 February 2026)

We theoretically study the effects of magnonic Kerr nonlinearity on magnon-polaritons (MPs) with a soft-mode in easy-axis ferromagnets coupled to a microwave cavity. Using an effective circuit model capable of describing MPs up to the nonperturbative strong-coupling regime, we show that chaotic and frequency-comb-like behaviors of MPs emerge at the original modes crossing point. Furthermore, we demonstrate that the Kerr nonlinearity induces a finite excitation gap in the soft-mode, particularly in the strong-coupling regime.

I. INTRODUCTION

Cavity magnonics, wherein the key excitation is a magnon-polariton (MP) that is a strongly coupled state of spin waves (magnons) and microwave photons, is one of the prominent platforms for novel quantum devices¹⁻³. In general, polariton states satisfying $g/\omega_{c(m)} \gtrsim 0.3$ are referred to as the *nonperturbative* strong-coupling (NSC) regime^{4,5}, where $\omega_{c(m)}$ denotes the characteristic angular frequency of the cavity or matter excitation and g is the coupling strength. In this regime, the excitation nonconserving nature of the light-matter interaction leads to strongly squeezed polariton states, giving rise to a nontrivial ground state characterized by virtual excitations and nonclassical correlations⁶.

Very recently, NSC has been experimentally demonstrated in MP systems based on superconductor/ferromagnet nanostructures^{7,8} and magnetic slab geometries⁹. Within cavity magnonics and linear spin-wave theory, perfect magnon squeezing has been predicted by exploiting soft-mode (zero-mode) magnons, whose excitation gap vanishes at the critical magnetic field¹⁰⁻¹². Typically, such soft-modes arise in anisotropic magnets with canted magnetization configurations induced by an external magnetic field applied perpendicular to the anisotropy axis^{13,14}. These magnetic anisotropies give rise to nonlinear magnon effects, the simplest of which is the self-Kerr nonlinearity¹⁵. Under sufficiently strong driving, the Kerr nonlinearity substantially modifies uniform magnon dynamics, leading to bistability¹⁶, frequency-comb generation¹⁷, and chaotic behavior^{18,19}. Therefore, it is highly desirable to reveal the effects of magnonic Kerr nonlinearity on the dynamics of MPs in the NSC regime.

In this paper, we theoretically investigate how the Kerr nonlinearity affect the dynamics of MPs with a soft-mode in easy-axis ferromagnets. Using an effective circuit model capable of describing MPs up to the NSC regime²⁰⁻²⁴, we show that chaotic and frequency-comb-like behaviors of MP at the original modes crossing point in the typical strong coupling (SC) regime with $g/\omega_{c(m)} \approx 0.01$. Furthermore, the Kerr nonlinearity induces a finite excitation gap in the soft-mode especially in the SC regime. In contrast, such nonlinear behaviors of

MPs are found to be strongly suppressed in the NSC regime characterized by $g/\omega_{c(m)} \approx 1$.

II. EFFECTIVE CIRCUIT MODEL OF MAGNON-POLARITONS

Based on our previous works²⁰⁻²⁴, we begin by reviewing the concept of an effective circuit model for cavity magnonics systems. As illustrated in Fig. 1 (a), the effective circuit represents the microwave photon system as a single *LC* resonator while the magnetization dynamics of an easy-axis ferromagnet inserted into the inductor correspond to the magnon system. Within the inductor, the magnetization of the ferromagnet is driven by the microwave magnetic field $\mathbf{H}(t)$ associated with the *LC* resonator mode. The microwave photons thereby couple to the magnon dynamics, $\mathbf{M}(t)$, through the electromagnetic interaction. The magnon dynamics is described by the Landau-Lifshitz-Gilbert (LLG) equation

$$\frac{d\mathbf{M}}{dt} = -\gamma\mathbf{M} \times \left(-\frac{\delta U_m}{\delta \mathbf{M}} + \mu_0 k_c \mathbf{H}(t) \right) + \frac{\alpha}{M_s} \mathbf{M} \times \frac{d\mathbf{M}}{dt}, \quad (1)$$

where M_s is the saturation magnetization of a ferromagnet, γ is the gyromagnetic ratio, k_c is the effective Nagaoka coefficient of an inductor, which is responsible for the mode volume of the microwave photon, μ_0 is the permeability of free space, and α is the Gilbert damping constant. Here, the total magnetic energy is assumed to be

$$U_m = -\mu_0 \mathbf{M} \cdot \mathbf{H}_0 - \frac{1}{2} \mu_0 \mathbf{M} \cdot \mathbf{H}_d[\mathbf{m}], \quad (2)$$

where $\mathbf{H}_0 = H_0 \hat{\mathbf{z}}$ is the external static magnetic field and $\mathbf{H}_d[\mathbf{m}] = -M_s(m_y \hat{\mathbf{y}} + m_z \hat{\mathbf{z}})/2$ describes the demagnetization field due to a cylindrical rod shape of a ferromagnet. Here, $\mathbf{m}(t) = \mathbf{M}(t)/M_s = (m_x, m_y, m_z)$ is the unit vector along the magnetization direction of the ferromagnet. Introducing the polar angle $\theta(t)$ and azimuthal angle $\varphi(t)$ for $\mathbf{m}(t) = (\cos \varphi \sin \theta, \sin \varphi \sin \theta, \cos \theta)$, Eq. (2) can be expressed as

$$\frac{U_m}{\mu_0 M_s^2} = -\frac{H_0}{M_s} \cos \theta + \frac{1}{4} (1 - \cos^2 \varphi \sin^2 \theta), \quad (3)$$

which gives the equilibrium position of $\mathbf{m}(t \rightarrow \infty)$ in the absence of $\mathbf{H}(t)$ by $(\theta_\infty, \varphi_\infty) = (\cos^{-1}(2H_0/M_s), 0)$. Note

^{a)}Electronic mail: t.chiba@yz.yamagata-u.ac.jp

that a strong field, $H_0 \geq M_s/2$, aligns the magnetization along the z direction, resulting in $\theta_\infty = 0$ whereas a weaker field, $H_0 < M_s/2$, produces canted magnetization configurations with two degenerate equilibrium positions at $\varphi_\infty = 0$ [see Fig. 1 (b)]. In the XYZ -coordinate system depicted in Fig. 1 (a), the magnetization is stabilized along the Z -axis determined by θ_∞ and φ_∞ . Denoting the transformation matrix as $\mathcal{R}(\theta_\infty)$ around the $Y(y)$ -axis, in the presence of $\mathbf{H}(t)$, the magnetization $\mathbf{n}(t) = \mathcal{R}(\theta_\infty)\mathbf{m}(t) = (n_X, n_Y, n_Z)$ precesses around $\mu_0\mathbf{H}_R = \mathcal{R}(\theta_\infty)(-\delta U_m/\delta \mathbf{M})$. For a small microwave field $\mathbf{p}(t) = \mathcal{R}(\theta_\infty)\mathbf{h}(t)$ given by $\mathbf{h}(t) = \mathbf{H}(t)/M_s$, the magnetization dynamics can be linearized as $\dot{\mathbf{n}}(t) = (n_X(t), n_Y(t), 1)$ with $|n_X|, |n_Y| \ll 1$. Therefore, the linearized LLG equation gives the magnon eigenfrequency

$$\omega_m = \begin{cases} \gamma' \mu_0 \sqrt{(M_s/2)^2 - H_0^2} & (H_0 < M_s/2) \\ \gamma' \mu_0 \sqrt{H_0 (H_0 - M_s/2)} & (H_0 \geq M_s/2) \end{cases}, \quad (4)$$

where $\gamma' = \gamma/\sqrt{1 + a^2}$. At $H_0 = M_s/2$, the magnon eigenfrequency once becomes zero, indicating the presence of soft magnons¹².

Next, we investigate eigenmodes of MP in the framework of the effective circuit model. Inside the inductor, the microwave field is induced by an alternating current $I(t)$ via Ampère's law: $\mathbf{H}(t) = (NI(t)/l)\hat{\mathbf{x}}$, where N is a turn number and l is the inductor length. Defining the circuit mode angular frequency by $\omega_c = 1/\sqrt{LC}$ with an inductance L and an electrostatic capacitance C , the dynamics of the microwave field is governed by^{23,24}

$$\left(\frac{d^2}{dt^2} + 2\beta\omega_c \frac{d}{dt} + \omega_c^2 \right) \mathbf{H} + k_m \eta_s \frac{d^2 \mathbf{M}}{dt^2} = \omega_c^2 \mathbf{H}_V(t), \quad (5)$$

where $\beta = R\sqrt{C/L}/2$ is an effective damping of the circuit with an electrical resistance R , k_m is the effective Nagaoka coefficient of a ferromagnet, η_s ($0 \leq \eta_s \leq 1$) represents the volume ratio between the inductor and ferromagnet, and $\mathbf{H}_V(t)$ ($\mathbf{p}_V(t) = \mathcal{R}(\theta_\infty)\mathbf{H}_V(t)/M_s$ in the XYZ -coordinate) is a driving magnetic field from the source. Assuming harmonic solutions $p_X(t) = \tilde{p}_X e^{-i\omega t}$ and $n_X(t) = \tilde{n}_X e^{-i\omega t}$ for the input $p_V(t) = p_V e^{-i\omega t}$, we obtain the coupled equations in the frequency domain^{23,24}

$$\bar{\Omega} \begin{pmatrix} \tilde{p}_X \\ \tilde{n}_X \end{pmatrix} = \begin{pmatrix} -\omega_c^2 p_V \\ -\omega_{||1} \omega_\perp \end{pmatrix} \quad (6)$$

with

$$\bar{\Omega} = \begin{pmatrix} \omega^2 + 2i\beta\omega_c\omega - \omega_c^2 & k_m \eta_s \cos^2 \theta_\infty \omega^2 \\ k_c \gamma' \mu_0 M_s \omega_{||1} & \omega^2 + 2i\alpha_m \omega_m \omega - \omega_m^2 \end{pmatrix}, \quad (7)$$

where $\alpha_m = \alpha(\omega_{||1} + \omega_{||2})/2/\sqrt{1 + \alpha^2}/\omega_m$, $\omega_{||1} = \gamma' \mu_0 (H_0 \cos \theta_\infty + M_s \sin^2 \theta_\infty/2)$, $\omega_{||2} = \gamma' \mu_0 (H_0 \cos \theta_\infty - M_s \cos 2\theta_\infty/2)$, and $\omega_\perp = \gamma' \mu_0 (-H_0 \sin \theta_\infty + M_s \sin 2\theta_\infty/4)$. In order to obtain the eigenfrequency of the hybridized MP modes, we neglect the damping parameters in Eq. (7) by setting $\alpha_m = \beta = 0$. Then, hybridized eigenmodes ω_\pm are calculated by solving the

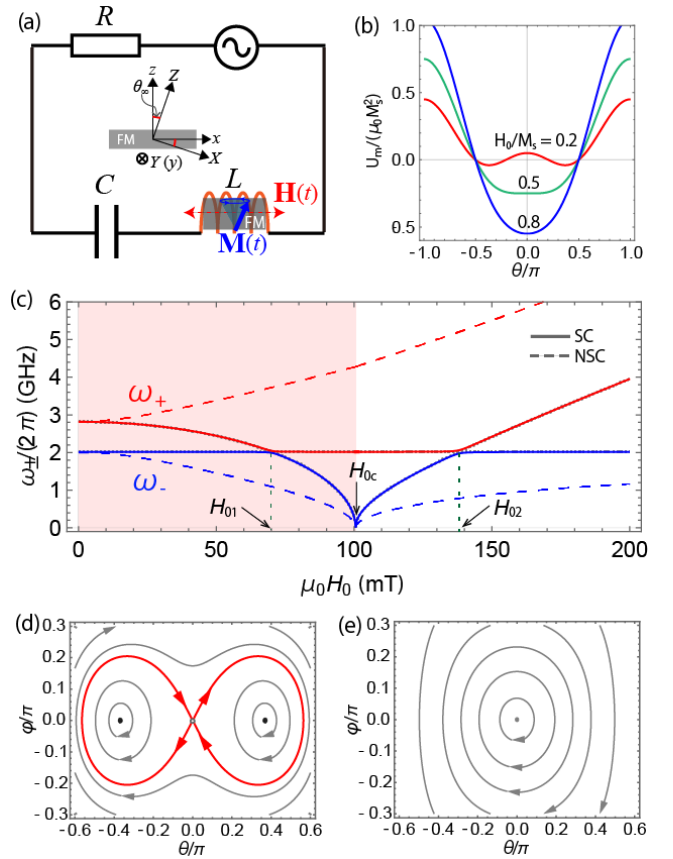


FIG. 1. (a) Effective circuit model of a cavity magnonics system, where $\mathbf{M}(t)$ represents the uniform magnetization dynamics (magnons) in an easy-axis ferromagnet (FM) and $\mathbf{H}(t)$ denotes the microwave magnetic field (photons) in the inductor. The equilibrium magnetization is characterized by the angle θ_∞ measured from the z axis. (b) Total magnetic energy U_m as a function of the polar angle θ at $\varphi = 0$ for different values of H_0/M_s . (c) Eigenfrequencies (ω_\pm) of MPs as a function of the external magnetic field ($\mu_0 H_0$) for different ratios of d_M/d : SC for $d_M/d = 0.02$ and NSC for $d_M/d = 1$. The critical field $H_{0c} = M_s/2$ marks the transition of the equilibrium magnetization position. (d),(e) Phase portraits for (b), where the red line, filled circles, and open circle denote the homoclinic orbit, centers, and saddle point, respectively: (d) $H_0 < H_{0c}$ and (e) $H_0 > H_{0c}$.

determinant of Eq. (7). Accordingly, the coupling strength at the original modes crossing point ($\omega_m = \omega_c$) is given by

$$g \equiv \left. \frac{\omega_+ - \omega_-}{2} \right|_{\omega_m = \omega_c}. \quad (8)$$

In this paper, we assume circular cross sections for both the inductor and the ferromagnet, characterized by d and d_M as the diameters of the inductor and ferromagnet, respectively. Then, we have the volume ratio factor $\eta_s = d_M^2/d^2$. We use circuit parameters: $L = 6.2$ nH (for $N = 5$, $l = 15$ mm, and $d = 2$ mm), $C = 1$ pF, and $R = 1$ Ω , which corresponds to $k_c = 0.947$, $\omega_c/(2\pi) = 2.0$ GHz, and $\beta = 6.3 \times 10^{-3}$. For simplicity, $k_m = k_c$ is assumed. By assuming $\text{Y}_3\text{Fe}_5\text{O}_{12}$, we also use material parameters: $\gamma = 1.76 \times 10^{11}$ T $^{-1}$ s $^{-1}$, $\alpha = 10^{-4}$, and $M_s = 1.6 \times 10^5$ Am $^{-1}$ ^{22,25}.

To investigate how the system damping (α_m , β) affect the hybridized MP modes²⁴, we discuss eigenfrequencies of the MP modes for $d_M/d = 0.02$ and $d_M/d = 1$, which are displayed in Fig. 1 (c). For $d_M/d = 0.02$, we have coupling ratios: $g/\omega_c = 0.01$ at H_{01} and $g/\omega_c = 0.02$ at H_{02} . Here, $H_{01} = 70$ mT and $H_{02} = 138$ mT are values of the external magnetic field at each original mode crossing point, which are shown in Fig. 1 (c). At these two points, the condition of $g/\omega_c > \alpha_m, \beta$ but $g/\omega_c < 0.1$ indicate that the MPs for $d_M/d = 0.02$ reside in the SC regime. In contrast, for $d_M/d = 1$, we have coupling ratios: $g/\omega_c = 0.65$ at H_{01} and $g/\omega_c = 1.1$ at H_{02} , indicating that they reach the NSC regime.

III. MAGNONIC KERR NONLINEARITY AND DUFFING MODEL

Here, we discuss the nonlinear effects on the dynamics of MPs. To elucidate the origin of these effects, we first consider an extreme case of the magnon dynamics: a very weak external field, $H_0 \ll M_s/2$, is applied to the z direction in Fig. 1 (a). In this limit, the magnetic anisotropy (demagnetization field) term in Eq. (2) dominates the total magnetic energy, which can be approximated as $U_m \approx \mu_0 M_s^2 (1 - m_x^2)/4$. Defining the transverse magnetization (magnon) as $m_\perp = m_y + im_z$ and employing a second-order approximation, $m_x \approx 1 - |m_\perp|^2/2$, Eq. (1) can be written in the following approximate form:

$$\frac{dm_\perp}{dt} \approx i \frac{\gamma \mu_0 M_s}{2} m_\perp - i \frac{\gamma \mu_0 M_s}{4} |m_\perp|^2 m_\perp, \quad (9)$$

in which the coupling term to photons and the Gilbert damping term are not displayed for simplicity. Equation (9) indicates that the full LLG equation with the total magnetic energy in Eq. (2) exhibits features of a Duffing oscillator^{19,26,27}, characterized by the anharmonic force $\sim x^3$, where x denotes the canonical position. The Duffing oscillator exhibits an amplitude-dependent frequency, which corresponds to the Kerr nonlinearity²⁸. Accordingly, in Eq. (9), the nonlinear frequency shift proportional to $|m_\perp|^2$ can be interpreted as the magnonic analog of the Kerr nonlinearity²³. We note, however, that this analytical correspondence between the LLG and Duffing equations²⁶ is generally valid only in special cases^{23,29}.

A global correspondence between the LLG equation and the Duffing equation at the topological level has recently been demonstrated in our previous work²⁷. This correspondence is established based on the nature of equilibrium points and the existence of homoclinic orbits, analyzed via linear stability analysis of the LLG equation. Similar to the Duffing oscillator, the presence of a pair of homoclinic orbits in the phase portraits is associated with the emergence of chaos in the magnetization dynamics²⁷. Following the same approach, Figs. 1 (d) and (e) summarize the global correspondence between Eq. (1) and the Duffing equation in terms of phase portraits. Note that, since the Kerr nonlinearity originates purely from the magnetic energy, the coupling to photons and the Gilbert damping term are neglected. Roughly speaking, these phase portraits correspond to the isoenergetic

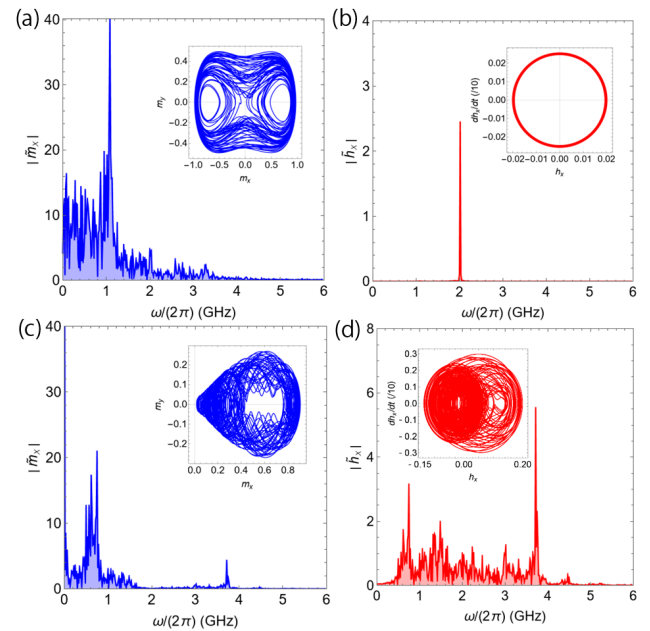


FIG. 2. Fourier spectra of (a) magnon and (b) photon dynamics at $H_0 = H_{01}$ for the SC case with $d/d_M = 0.02$. (c),(d) Fourier spectra for the NSC case with $d/d_M = 1$. Insets show the corresponding phase-space trajectories of the magnon and photon dynamics. Calculations are performed with the initial conditions $h_x(0) = 0.02$ and $m_x(0) = 0$ under $\mathbf{H}_V(t > 0) = \mathbf{0}$. The Fourier spectra are obtained from the dynamics in the time window $t = 440\text{--}500$ ns.

curves of Eq. (3). Figure 1 (d) shows that two distinct homoclinic orbits emanate from the same saddle point and enclose each center in a butterfly-like shape, indicating that the topology of the phase portrait is identical to that of the Duffing oscillator²⁷. It is worth noting that horseshoe chaos can arise when a homoclinic orbit exists in the phase space³⁰. In contrast, as seen in Fig. 1 (e), the homoclinic orbits vanish while the phase portraits remain anisotropic due to the Kerr nonlinearity (magnetic anisotropy). We also note that the MP system described by Eqs. (1) and (5) (for $\mathbf{H}_V(t) = \mathbf{0}$) is mathematically a fourth-order autonomous dynamical system, whose phase-space topology is similar to that of the Hénon-Heiles system^{31,32}.

IV. NUMERICAL DEMONSTRATION

Since we are interested in the influence of the Kerr nonlinearity on the hybridized MP modes shown in Fig. 1(c), we focus on the Hamiltonian dynamics of MPs by setting $\alpha = \beta = 0$ in Eqs. (1) and (5). We then compute the free oscillations of MPs at the original modes crossing points ($H_0 = H_{01}, H_{02}$) as well as at the critical field of the soft magnons ($H_0 = H_{0c}$). Without loss of generality, we consider the SC case with $d_M/d = 0.02$ (corresponding to $g/\omega_c \approx 0.01$) and the NSC case with $d_M/d = 1$ ($g/\omega_c \approx 1$).

A. Mode crossing point: $H_0 = H_{01}$

We compute the dynamics of MPs at $H_0 = H_{01}$, corresponding to the phase portraits containing the homoclinic orbit [see Fig. 1 (d)]. Figures 2 (a) and (b) show the Fourier spectra of the magnon (m_x) and photon (h_x) dynamics for the SC case with $d/d_M = 0.02$, where m_x and h_x denote the x -components of $\mathbf{m}(t) = \mathbf{M}(t)/M_s$ and $\mathbf{h}(t) = \mathbf{H}(t)/M_s$, respectively. As seen, the Fourier spectrum of magnons is broad and the magnetization trajectory covers a wide area in phase space [see inset]. Moreover, the magnon dynamics exhibits a strange-attractor-like trajectory, closely resembling the chaotic magnetization dynamics reported in our previous work²⁷. In contrast, the Fourier spectrum of photons shows an almost single peak and the Rabi-like splitting in Fig. 1 (c) appears to be suppressed by the Kerr nonlinearity²³, with the corresponding trajectory remaining closed (periodic) in phase space [see inset]. In addition, for $d/d_M = 0.02$, the photon system volume is much larger than that of magnons so that the photon dynamics is only weakly affected by the magnon dynamics. These observations indicate that the MPs are effectively decoupled. Then, we can treat the MP as a unidirectional coupling scheme³³ and effectively identify the current system with the third-order autonomous dynamical system composed of driven magnons²⁷.

Figures 2 (c) and (d) show the Fourier spectra of magnon and photon dynamics for the NSC case with $d/d_M = 1$. Both spectra are broad although the Rabi-like splitting in Fig. 1 (c) is still slightly visible. This result is in sharp contrast to the SC case, indicating that MPs persist in the NSC regime even in the presence of the Kerr nonlinearity. Moreover, the photon dynamics exhibits a strange-attractor-like trajectory covering a wide area in phase space, which may have potential applications in secure communication. These observations indicate that the system is a four-order autonomous dynamical system composed of MPs. Unlike our previous work²⁷ (or the SC case above) involving third-order chaos, the additional dimensionality due to the photon system may complicate the mathematical interpretation of chaos, potentially leading to hyperchaos³⁴, which is beyond the scope of this paper.

B. Mode crossing point: $H_0 = H_{02}$

We compute the dynamics of MPs at $H_0 = H_{02}$, corresponding to the phase portraits in Fig. 1 (e). Figures 3 (a) and (b) show the Fourier spectra of magnon and photon dynamics for the SC case with $d/d_M = 0.02$. As seen, the Fourier spectrum of magnons (m_x) exhibits comb-like frequency sidebands. In contrast, similar to the case of $H_0 = H_{01}$, the Fourier spectrum of photons shows an almost single peak and the Rabi-like splitting is absent. To facilitate the discussion of frequency-sideband generation, we label the positions of the main mode (ω_0) and the sidebands by ω_n ($n = -2, \dots, 3$), as shown in Fig. 3 (a). The frequency differences are defined as $\Delta_n/(2\pi) = \omega_{n+1}/(2\pi) - \omega_n/(2\pi)$. These values satisfy $\Delta_{-2}/(2\pi) = \dots = \Delta_2/(2\pi) \approx 0.34$ GHz, which corresponds to the main peak ($\omega_z/(2\pi) = 0.34$ GHz) of the Fourier spectrum of m_z arising from the Kerr nonlinearity²³. Thus, the fre-

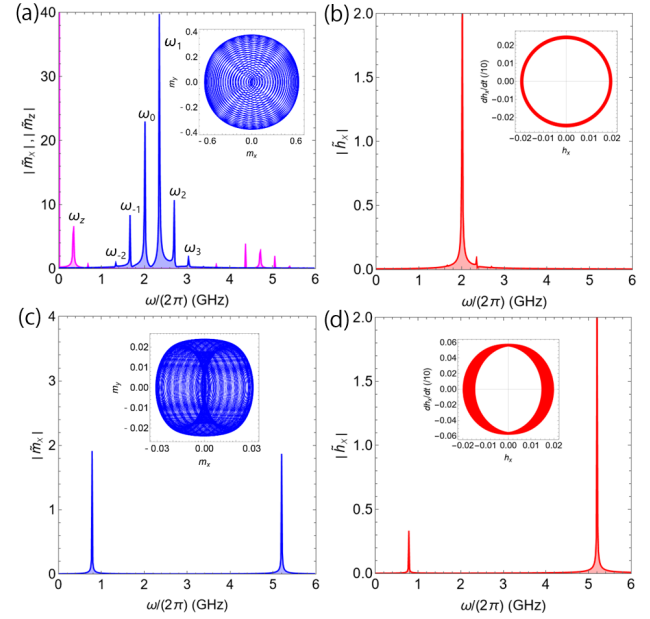


FIG. 3. Fourier spectra of (a) magnon and (b) photon dynamics at $H_0 = H_{02}$ for the SC case with $d/d_M = 0.02$. The Fourier spectrum of m_z is shown in magenta. (c),(d) Fourier spectra for the NSC case with $d/d_M = 1$. Insets show the corresponding phase-space trajectories of the magnon and photon dynamics. Calculations are performed under the same conditions as in Fig. 2.

quency sidebands can be interpreted as resulting from sum- and difference-frequency generation (superposition) between the main mode ($\omega_0 \approx \omega_m$) and the nonlinear mode (ω_z), expressed as

$$\omega_n = \omega_0 + n\omega_z \quad (n = -2, \dots, 3). \quad (10)$$

Figures 3 (c) and (d) show the Fourier spectra of magnon and photon dynamics for the NSC case with $d/d_M = 1$. As seen, the Rabi-like splitting is clearly visible in both spectra. The magnon dynamics exhibits quasi-periodic behavior. This result is in sharp contrast to the SC case, indicating that MPs robustly persist in the NSC regime.

C. Critical field point: $H_0 = H_{0c}$

We compute the dynamics of MPs at the critical field corresponding to the soft-mode ($H_0 = H_{0c}$). Figures 3 (a) and (b) show the Fourier spectra of magnon and photon dynamics for the SC case with $d/d_M = 0.02$. As seen, a finite excitation gap appears in the soft-mode of the magnon spectrum. This gap arises from the confinement effect due to the higher-order magnon potential, which is the origin of the Kerr nonlinearity.

Figures 4 (c) and (d) show the Fourier spectra for the NSC case with $d/d_M = 1$. The finite excitation gap in the soft-mode is suppressed. Furthermore, photons couple to the soft-mode magnons, resulting in Rabi-like splitting, in sharp contrast to the SC case. These observations indicate that MPs robustly persist in the NSC regime. In other words, the NSC regime

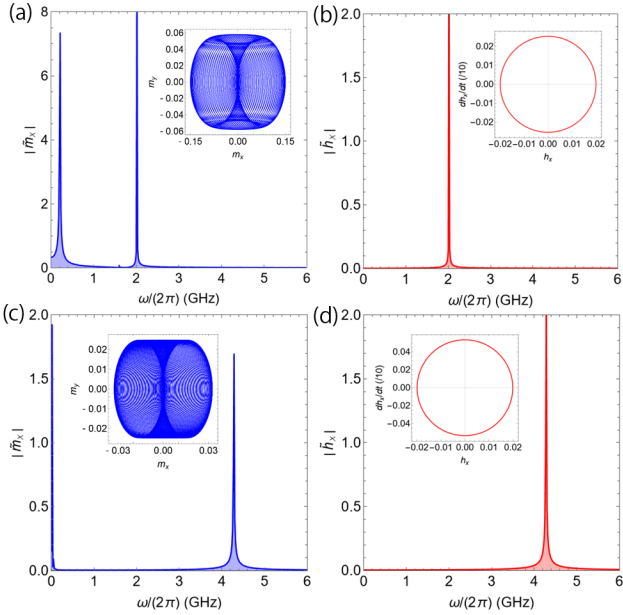


FIG. 4. Fourier spectra of (a) magnon and (b) photon dynamics at $H_0 = H_{0c}$ for the SC case with $d/d_M = 0.02$. (c),(d) Fourier spectra for the NSC case with $d/d_M = 1$. Insets show the corresponding phase-space trajectories of the magnon and photon dynamics. Calculations are performed under the same conditions as in Fig. 2.

overcomes the magnonic Kerr nonlinearity, which may support divergence-like behavior of quantum squeezing by exploiting the soft (zero)-mode magnons^{10,11} beyond the linear spin-wave approximation.

V. SUMMARY

In summary, we have theoretically investigated the influence of magnonic Kerr nonlinearity on hybridized MP modes with a soft-mode in easy-axis ferromagnets. Based on an effective circuit model capable of describing the NSC regime, we computed the dynamics of MPs at the original modes crossing points as well as at the critical field of soft magnons. We demonstrated that MPs exhibit chaotic and frequency-comb-like behaviors at the original modes crossing points in the typical SC regime ($g/\omega_{c(m)} \approx 0.01$). We also found that a finite excitation gap emerges in the soft-mode due to the Kerr nonlinearity, particularly in the SC regime. In contrast, such nonlinear behaviors are strongly suppressed in the NSC regime ($g/\omega_{c(m)} \approx 1$). This suppression supports the validity of the linear spin-wave approximation, which is essential for quantum squeezing using soft (zero)-mode magnons^{10,11}.

ACKNOWLEDGMENTS

The author thanks R. Tatsumi, R. Suzuki, H. Chiba, T. Taniguchi, and T. Oto for valuable discussions. This work was supported by Grants-in-Aid for Scientific research (Grants

No. 22K14591 and No. 25H02105).

DATA AVAILABILITY

The data that support the findings of this study are available from the corresponding author upon reasonable request.

- ¹B. Z. Rameshti, S. V. Kusminskiy, J. A. Haigh, K. Usami, D. L.-Quirion, Y. Nakamura, C.-M. Hu, H. X. Tang, G. E. Bauer, and Y. M. Blanter, Cavity magnonics, *Phys. Rep.* **979**, 1 (2022).
- ²H.Y. Yuan, Y. Cao, A. Kamra, R. A. Duine, P. Yan, Quantum magnonics: when magnon spintronics meets quantum information science, *Phys. Rep.* **965**, 26 (2022).
- ³Y. Li, W. Zhang, V. Tyberkevych, W.-K. Kwok, A. Hoffmann, and V. Novosad, Hybrid magnonics: Physics, circuits, and applications for coherent information processing, *J. Appl. Phys.* **128**, 130902 (2020).
- ⁴P. F.-Díaz, L. Lamata, E. Rico, J. Kono, and E. Solano, Ultrastrong coupling regimes of light-matter interaction, *Rev. Mod. Phys.* **91** 025005 (2019).
- ⁵A. F. Kockum, A. Miranowicz, S. D. Liberato, S. Savasta, and F. Nori, Ultrastrong coupling between light and matter, *Nat. Rev. Phys.* **1**, 19 (2019).
- ⁶A. Baydin, H. Zhu, M. Bamba, K. R. A. Hazzard, and J. Kono, Perspective on the quantum vacuum in matter, *Opt. Mater. Express* **8**, 1833 (2025).
- ⁷I. A. Golovchanskiy, N. N. Abramov, V. S. Stolyarov, M. Weides, V. V. Ryazanov, A. A. Golubov, A. V. Ustinov, and M. Y. Kupriyanov, Ultrastrong photon-to-magnon coupling in multilayered heterostructures involving superconducting coherence via ferromagnetic layers, *Sci. Adv.* **7**, eabe8638 (2021).
- ⁸I. Golovchanskiy, N. N. Abramov, V. S. Stolyarov, A. A. Golubov, M. Yu. Kupriyanov, V. V. Ryazanov, and A. V. Ustinov, Approaching deep-strong on-chip photon-to-magnon coupling, *Phys. Rev. Appl.* **16**, 034029 (2021).
- ⁹G. Bourcin, J. Bourhill, V. Vlaminck, and V. Castel, Strong to ultrastrong coherent coupling measurements in a YIG/cavity system at room temperature, *Phys. Rev. B* **107**, 214423 (2023).
- ¹⁰J. M. Lee, H.-W. Lee, and M.-J. Hwang, Cavity magnonics with easy-axis ferromagnets: Critically enhanced magnon squeezing and light-matter interaction, *Phys. Rev. B* **108**, L241404 (2023).
- ¹¹M. Silaev, Ultrastrong magnon-photon coupling, squeezed vacuum, and entanglement in superconductor/ferromagnet nanostructures, *Phys. Rev. B* **107**, L180503 (2023).
- ¹²G. E. W. Bauer, P. Tang, M. Elyasi, Y. M. Blanter, and B. J. van Wees, Soft magnons in anisotropic ferromagnets, *Phys. Rev. B* **108**, 064431 (2023).
- ¹³S. Iihama, S. Mizukami, H. Naganuma, M. Oogane, Y. Ando, and T. Miyazaki, Gilbert damping constants of Ta/CoFeB/MgO(Ta) thin films measured by optical detection of precessional magnetization dynamics, *Phys. Rev. B* **89**, 174416 (2014).
- ¹⁴D. K. de Wal, A. Iwens, T. Liu, P. Tang, G. E. W. Bauer, and B. J. van Wees, Long distance magnon transport in the van der Waals antiferromagnet CrPS4, *Phys. Rev. B* **107**, L180403 (2023).
- ¹⁵S. Zheng, Z. Wang, Y. Wang, F. Sun, Q. He, P. Yan, and H. Y. Yuan, Tutorial: Nonlinear magnonics, *J. Appl. Phys.* **134**, 151101 (2023).
- ¹⁶Y.-P. Wang, G.-Q. Zhang, D. Zhang, T.-F. Li, C.-M. Hu, and J. Q. You, Bistability of cavity magnon polaritons, *Phys. Rev. Lett.* **120**, 057202 (2018).
- ¹⁷M. Wang, C. Kong, Z.-Y. Sun, D. Zhang, Y.-Y. Wu, and L.-L. Zheng, Nonreciprocal high-order sidebands induced by magnon Kerr nonlinearity, *Phys. Rev. A* **104**, 033708 (2021).
- ¹⁸B. Wang, C. Kong, Z.-X. Liu, H. Xiong, and Y. Wu, Magnetic-field-controlled magnon chaos in an active cavity-magnon system, *Laser Phys. Lett.* **16**, 045208 (2019).
- ¹⁹M. Elyasi, Y. M. Blanter, and G. E. W. Bauer, Resources of nonlinear cavity magnonics for quantum information, *Phys. Rev. B* **101**, 054402 (2020).
- ²⁰T. Chiba, T. Komine, and T. Aono, Ultrastrong-coupled magnon-polariton in a dynamical inductor based on magnetic-insulator/topological-insulator bilayers, *Appl. Phys. Lett.* **124**, 012402 (2024).
- ²¹T. Chiba, T. Komine, and T. Aono, Microwave Transmission Theory for On-Chip Ultrastrong-Coupled Magnon-Polariton in Dynamical Inductors, *J. Mag. Soc. Jpn.* **48**, 21 (2024).

²²K. Mita, T. Chiba, T. Kodama, T. Ueda, T. Nakanishi, K. Sawada, S. Tomita, Ultrastrongly coupled and directionally nonreciprocal magnon polaritons in magnetochiral metamolecules, *Phys. Rev. Appl.* **23**, L011004 (2025).

²³R. Suzuki, T. Chiba, and H. Matsueda, Gain-driven magnon-polariton dynamics in the ultrastrong coupling regime: Effective circuit approach for coherence versus nonlinearity, *Phys. Rev. B* **113**, 024412 (2026).

²⁴T. Chiba, R. Suzuki, T. Otaki, and H. Matsueda, Circuit-based cavity magnonics in the ultrasrtong and deep-strong coupling regimes, *Phys. Rev. B* **112**, 174403 (2025).

²⁵L. Bai, M. Harder, Y. P. Chen, X. Fan, J. Q. Xiao, and C.-M. Hu, Spin Pumping in Electrodynamically Coupled Magnon-Photon Systems, *Phys. Rev. Lett.* **114**, 227201 (2015).

²⁶S. H. Strogatz, *Nonlinear Dynamics and Chaos: With Applications to Physics, Biology, Chemistry, and Engineering* (Second Edition) (CRC Press, Boca Raton, 2015).

²⁷R. Tatsumi, T. Chiba, T. Komine, and H. Matsueda, Chaotic magnetization dynamics in magnetic Duffing oscillator, *Phys. Rev. E* **111**, 064202 (2025).

²⁸C. Zhang, M. Kim, J. Wang, and C.-M. Hu, Van der Pol-Duffing oscillator and its application to gain-driven light-matter interaction, *Phys. Rev. Appl.* **22**, 014034 (2024).

²⁹Y. M. Shukrinov, I. R. Rahmonov, A. Janalizadeh, and M. R. Kolahchi, “Anomalous Gilbert damping and Duffing features of the superconductor-ferromagnet-superconductor φ_0 Josephson junction,” *Phys. Rev. B* **104**, 224511 (2021).

³⁰S. Wiggins and M. Golubitsky, *Introduction to Applied Nonlinear Dynamical Systems and Chaos* (Springer, New York, 2003).

³¹M. Hénon and C. Heiles, The applicability of the third integral of motion, Some numerical experiments, *Astron. J.* **69**, 73 (1964).

³²S. Kaspereczuk, Homoclinic chaos in generalized Henon-Heiles system, *Acta phys. Pol., A* **88**, 1073 (1995).

³³Y. S. Gui and C.-M. Hu, Transient response of a gain-driven polariton, *Phys. Rev. Appl.* **21**, 044023 (2024).

³⁴S. T. Tanekou, J. Ramadoss, J. Kengne, G. D. Kenmoe, and K. Rajagopal, Coexistence of Periodic, Chaotic and Hyperchaotic Attractors in a System Consisting of a Duffing Oscillator Coupled to a van der Pol Oscillator, *Int. J. Bifurcation and Chaos* **33**, 2330004 (2023).